

EERA DeepWind'2014, 11th Deep Sea Offshore Wind R&D Conference

A comparison of LiDAR and radiosonde wind measurements

Valerie-M. Kumer^a, Joachim Reuder^a, Birgitte R. Furevik^{a,b}

^a*Geophysical Institute, University of Bergen, Allegaten 70, 5007 Bergen, Norway*

^b*Norwegian Meteorological Institute, Allegaten 70, 5007 Bergen, Norway*

Abstract

Doppler LiDAR measurements are already well established in the wind energy research and their accuracy has been tested against met mast data up to 100 m above ground. However, the new generation of scanning LiDAR have a much higher range and thus it is not possible to verify measurements at higher altitudes. Therefore, the LiDAR Measurement Campaign Sola (LIMECS) was conducted at the airport of Stavanger from March to August 2013 to compare LiDAR and radiosonde winds. It was a collaborative test campaign between the University of Bergen, the Norwegian Meteorological Office (MET), Christian Michelsen Research (CMR) and Avinor. With the airports' location at the Norwegian West Coast, additional motivations were the investigations in characteristics of coastal winds, as well as the validation of the LES turbulence forecast for the airport of Stavanger. We deployed two Windcubes v1 and a scanning Windcube 100S at two different sites in Sola, one next to the runway and the other one near to the autsonde from MET. The Windcube 100S scans several cross-sections of the ambient flow on hourly basis. In combination with wind profiles up to 200 m (Windcubes v1) and 3 km (Windcube 100S) and temporally more frequent radiosonde ascents, we collect a variety of wind information in the coastal atmospheric boundary layer. First results show increasing correlation of 0.95 to 0.99 for increasing measurement heights (125 to 1325 m) between the scanning LiDAR wind profiles and the radiosonde horizontal wind speeds. Though the number of LiDAR measurements decreases with increasing height, the measurements seem to correlate better with the radiosonde data in high altitudes.

© 2014 Elsevier Ltd. This is an open access article under the CC BY-NC-ND license

(<http://creativecommons.org/licenses/by-nc-nd/3.0/>).

Selection and peer-review under responsibility of SINTEF Energi AS

Keywords: LiDAR, rawinsonde, planetary boundary layer

1. Introduction

The development of LiDAR technology over the last decades now provides the atmospheric boundary layer community with new instrumentation for studying the ambient flow field. One important driver of this development is the wind energy sector. The continuously increasing size of wind turbines has been pushing a demand for replacement and complementation of static meteorological mast measurements. The now commercially available LiDAR wind profilers with a typical measurement range of 200 m above ground, have during the last years proven their capabil-

* Valerie-M. Kumer. Tel.: +47-55-58-2672.

E-mail address: valerie.kumer@gfi.uib.no

ity of measuring the wind speed and turbulence intensity with an accuracy comparable to the well established cup anemometers, at least over not too complex terrain [1].

The new generation of scanning LiDAR enable not only a visualization of the ambient flow field by scanning two-dimensional vertical or horizontal cross sections but also show a higher range. Scanning in 2D makes new measurement strategies possible and opens a new way of analysing boundary layer structures as well interacting processes as wind turbine wakes. However, the access to higher wind measurements requires new validation methods as the measurement range exceeds the one of meteorological masts. Therefore the University of Bergen conducted in collaboration with the Norwegian Center of Offshore Wind Energy (NORCOWE) and the Norwegian Meteorological Institute (MET) the LiDAR Measurement Campaign Sola (LIMECS) in order to investigate coastal boundary layer processes and to compare scanning LiDAR and Radiosonde wind profiles.

A Radiosonde is a rising weather balloon equipped with a GPS antenna and sensors for temperature, humidity and pressure measurements. Radiosondes have been used since the 20ies to measure profiles throughout the whole atmosphere and are now operated daily of Meteorological Institutes all over the world. Radiosonde data are distributed internationally through the global telecommunication system (GTS) for assimilation into weather forecast models. Nowadays, the radiosondes in Sola are released automatically by a so-called autosonde. It is located near the airport of Stavanger on the west coast of Norway (figure 1).

Operating a scanning LiDAR at the Norwegian coast allowed us to additionally investigate boundary layer transition processes from the boundary layer over sea to the one over land. One of this processes, which is also dominant in coastal climates is the land-sea breeze circulation. It is generated by solar radiation and the different heat capacities of the sea and terrestrial areas. In the later case study of a land breeze the sea is warmer than the land, leading to warmer, rising air over the sea. Due to pressure differences the rising air is directed towards the land, where it is sinking again, leading to a closed circulation. According to cases studied by Oke, the average land breeze is not as strong as the sea breeze with velocities of 1-2 m/s and a depth of around 300 m, compared to 2-5 m/s and 1-2 km for the sea breeze [2]. The sea breeze circulations are of importance for offshore wind energy as they extend several tens of kilometres offshore and reduce offshore wind speeds relative to the coast line [3]. As sea breeze occurrences are linked to temperature gradients between land and sea, they not only alter the wind potential on a spatial scale but also introduce a seasonal wind speed variability, which should be taken into account for offshore wind energy assessment. Therefore, measurements capturing these events are useful for a better understanding of sea breeze characteristics and model validations.

Hooper and Eloranta already compared LiDAR and radiosonde boundary layer depth, wind and direction measurements back in the 80ies and concluded with a favourable comparison [4]. The presented study follows up on their results in greater detail and is structured as follows. Section 2 gives a short description of the LIMECS measurement campaign, followed by a presentation of the data and methods used in section 3. Section 4 presents and discusses the results of a comparison between the wind profiles measured by the Leosphere 100 S scanning wind LiDAR system and radiosondes up to an altitude of 2500 m above ground. Two case studies in section 5 shortly highlight the potential of 3D scanning LiDAR systems for various small scale boundary layer phenomena. Finally section 6 gives a summary and outlook on future activities.

2. Campaign Setup

LIMECS was set up at two sites at the airport of Stavanger in Sola and lasted from March 1st, 2013 with a duration of around four months until August 24th, 2013. The scanning WindCube (WLS100S-8) and a WindCube v1 (WLS7-67) measured wind fields and profiles from above the rooftop of the fire brigade building at Stavanger airport (site 1), respectively. The fire brigade building is located 1.7 km of the the Norwegian coast line. With that, the measurements were in general inside the transition zone between the maritime boundary layer and the one over land. Further inland and 2.3 km south-east of site 1 the second WindCube v1 (WLS7-65) measured wind profiles next to the autosonde operated by MET (site 2 in figure 1). During LIMECS we temporarily increased the radiosonde launches from 2 to 4 releases per day for interesting weather conditions, which can be seen in figure 2 as higher concentration of gray lines.

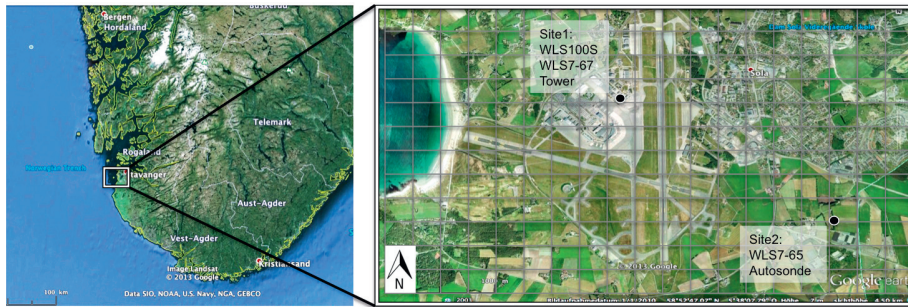


Fig. 1: Map of the LIMECS setup in the area around the airport of Stavanger in Sola, Norway. The black dots indicate the location of the two measurement sites.

54 3. Data and Methods

55 An autosonde manufactured by Vaisala and operated by MET Norway has its location in Sola (site 2 figure 1).
 56 The autosonde releases two radiosondes every day. Each balloon has a climbing speed of approximately 6 m/s and is
 57 equipped with a RS92-SGP radiosonde, also manufactured by Vaisala. The radiosonde has sensors for pressure, air
 58 temperature and relative humidity sensor, as well as a GPS on board. It uses the code correlation GPS technique to
 59 calculate the horizontal wind speed and direction from the position of the radiosonde and its relative motion towards
 60 the satellites, which is detected through the received Doppler frequency [5]. For that, the radiosonde needs at least
 61 four different satellite codes. The manufacturer's accuracy of this method to calculate wind speed and direction are
 62 listed in table 1 [6]. The radiosonde raw data has a sampling rate of two seconds, leading to a vertical measurement
 63 resolution of around 11 m.

Table 1: Measurement accuracies as given by the manufacturer

	wind speed [m/s]	wind direction [°]
WLS 100S	0.5	-
WLS v1 radiosonde	0.2 0.5	1.5 4 (for wind speeds above 3 m/s)

64 The two WindCubes v1 measured the three dimensional wind vector every 20 meters from 40 to 200 m with a 4
 65 second independent sampling rate. Compared to the WindCube v1, the WindCube 100S measured at higher ranges
 66 between 150 and 3000 m, with a probe length of 75 m. In addition to wind profiles, the WindCube 100S also measured
 67 vertical and horizontal cross-sections of radial wind fields in a repetitive scanning pattern of three 360° PPI scans and
 68 five 180° RHI scans. The manufacturer's wind speed and direction accuracies can be found in table 1 [7], [8].

69 Due to the fact that LiDAR measurements depend on the presence of small particles as backscatter targets, the
 70 data availability can be altered by low aerosol concentration in the lower atmosphere. Therefore, the measurements
 71 are sensitive to the planetary boundary layer height and with that to certain weather conditions. Figure 2 illustrates
 72 the Carrier to Noise Ratio (CNR) of the WindCube 100S as a function of height for the later analysed period. Data
 73 with CNR values below - 27 dB are discarded and not stored in the general data file. Noticeable is the common signal
 74 drop at around 1.5 km. This altitude could be linked to the average planetary boundary layer height at the site. The
 75 variation of the measurement range could go along with the variation of boundary layer depth. However, the analysis
 76 of the boundary layer height with Doppler LiDARs is still under development, compared to already good correlations
 77 of boundary layer height studies with elastic backscatter LiDAR [9]. Next to atmospheric conditions, technical issues
 78 can also lead to a lower data availability, as we had software issues during March and a problem with the power supply
 79 during spring time (figure 2).

80 In order to compare LiDAR and radiosonde profiles a best fit detection algorithm searched for the closest LiDAR
 81 profile at the time of the radiosonde launch, as well as the closed radiosonde measurement height to the LiDAR

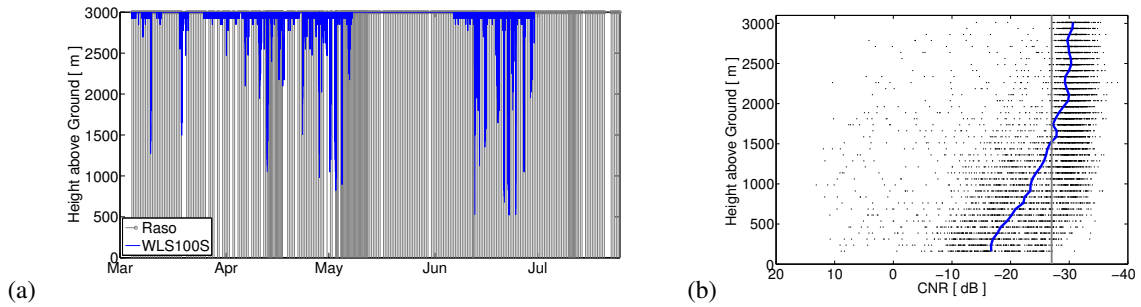


Fig. 2: (a) Data availability of WLS100S and radiosonde measurements over the whole measurement period. The blue lines indicate the maximal available measurement height; (b) LiDAR CNR values as a function of height for the common analysing period. The blue line indicates the average profile, while the gray line shows the programmed CNR threshold

82 heights. After that a 10 minute time average over the time fit and a 75 m average over the space fit lead to a set of
 83 profiles which are the core of this study. We calculated the standard deviation of the wind direction with the Yamartino
 84 method discussed by Tuner [10].

85 **4. Results**

86 Applying the previously discussed methods to the data of the WindCube 100S and the radiosonde in the period
 87 from March 1st to July 20th 2013, reveals overall high correlation ($R > 0.95$) between the two different measurement
 88 techniques (figure 3). The correlations are not constant, but dependent on the measurement height. In order to
 89 visualize this dependency, we plotted the correlation coefficients as a function of height (right hand side of figure 3).

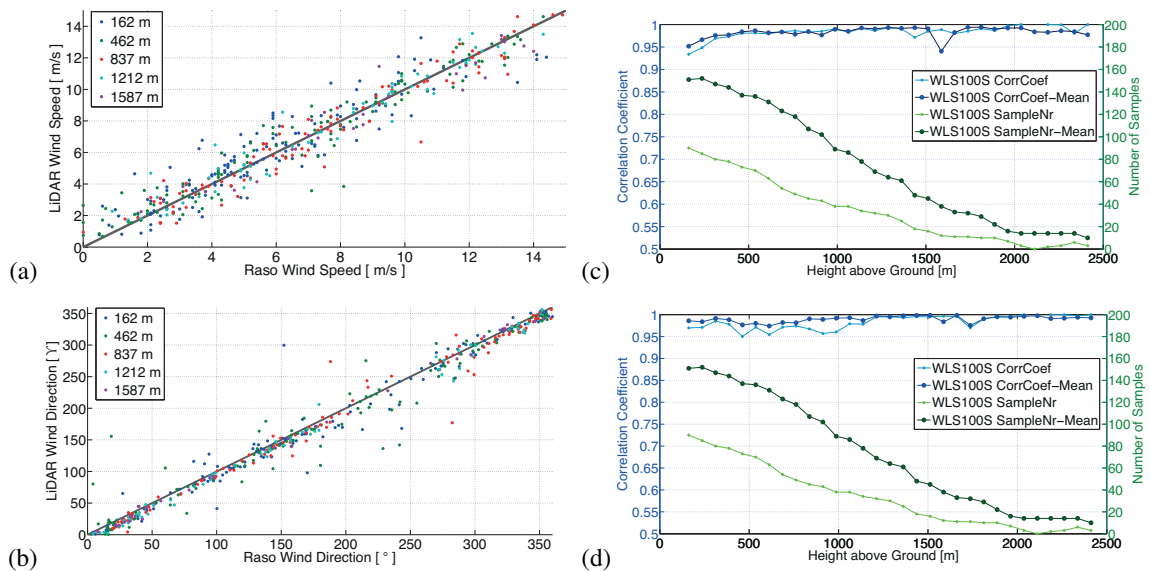


Fig. 3: Scatter plot of (a) horizontal wind speeds and (b) wind direction measured by the radiosonde and the WindCube 100S. The colors indicate different measurement heights; Correlation coefficients for (c) horizontal wind speed and (d) wind direction in blue and number of samples of the WindCube 100S in green are plotted as a function of height. Light colors indicate the best fit profiles, dark colors the time and space averaged data

90 The correlation coefficients clearly increase from $R = 0.93$ to $R = 0.99$ between 150 m and 500 m. After that,
 91 R is almost constant at around 0.99, even though the number of samples that are compared decreases (3c). When

92 averaging an ensemble of profiles five minutes before and after the closest LiDAR profile, not only the number of
 93 samples but also the correlations increases for most of the measurement heights. Averaging the wind direction is
 94 even more effective. A reason for the drop of the correlation coefficient at around 1.6 km could be due to the first
 95 LiDAR measurements after the cloud level, as their optical thickness influences the laser intensity and with that the
 96 LiDAR CNR. Compared to the WindCube 100S, correlations become worse between data from the WindCubes v1
 97 (figure 4) and Radiosonde measurements. In fact, the correlation coefficients are in the order of two tenths lower than
 98 correlations between the WindCube 100S and the Radiosonde. However, correlations to the Radiosonde still increases
 99 from $R = 0.7$ to $R = 0.9$ for the WLS7-67 and from $R = 0.6$ to $R = 0.7$ for the WLS7-65 for measurements heights at
 100 70 and 210 m respectively. It should be noted that the number of compared samples of the WLS7-65 is almost double
 101 as high as for the WindCube 100S. Limiting the WLS7-65 profiles to the ones used for the WLS 100S, we can at least
 102 compare wind speed measurements at around 230 m (figure 4). The correlation coefficient is with 0.842 higher than
 103 the correlation between the WLS7-65 and the radiosonde. However, the correlation between the WindCube 100S and
 104 the WLS7-65 at 230 m is still one tens lower than the correlation coefficient between the WindCube 100S and the
 105 radiosonde at the same height. Apart from different local effects that arise with the 2.3 km distance between the two
 106 LiDAR devices, the data quality of the WLS7-65 seems not to be influenced by an affected laser amplifier.

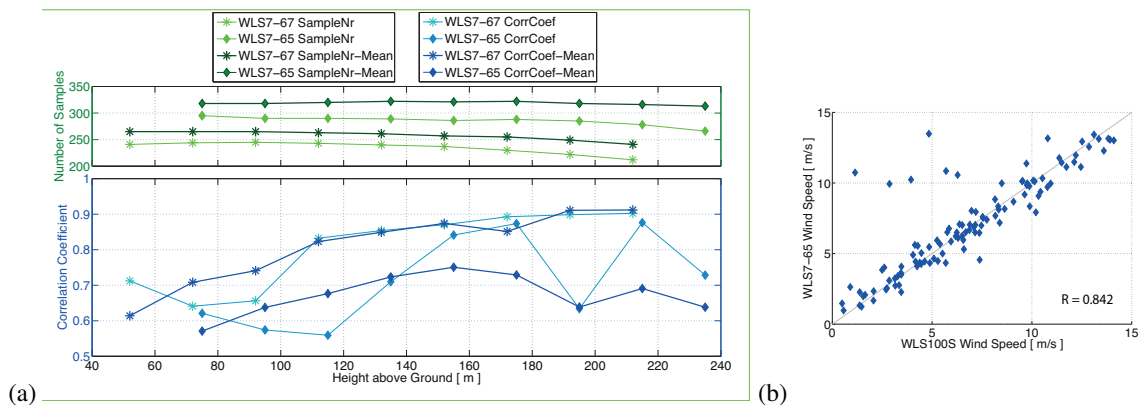


Fig. 4: (a) Correlation Coefficients between the WindCubes v1 and the Radiosonde for horizontal wind speed and number of samples are plotted as a function of measurement height in blue and green, respectively. Light colors indicate the results for the best fit profiles, while dark colors represent the time and space averaged data. Diamonds show the results for the WindCube WLS7-65, while stars represent results for the WindCube WLS7-67. (b) Scatter plot of horizontal wind speeds between the WindCube 100S and the WindCube WLS7-65 at 230 m.

107 The increased correlation between both LiDAR devices enforces the theory, that apart from the different length of
 108 the WLS7-65 data sets, the motion of the balloon could also influence the correlations. If there are a bit stronger winds,
 109 the balloon under which the radiosonde is attached gets some momentum when entering the atmosphere. Therefore
 110 the rope on which the radiosonde is attached starts to swing for some time while rising. When watching the ascent
 111 of the radiosonde, this pendulum like motion can be observed even with the eye. This motion can lead to inaccurate
 112 wind measurements at lower altitudes. Vaisala tries to account for this effect in their provided software.

113 4.1. Case Studies

114 To investigate the lower correlations at surface near levels, we show as a first case study two wind speed and
 115 direction profiles where the highest standard deviation in the spatial averaged radiosonde data is at first measurement
 116 altitudes (figure 5). Compared to this spatial variations, the standard deviations of the WindCube measurements
 117 represents variation within a 10 minutes time interval. In this case the standard deviations are higher in time than
 118 in space. Not only the size of the time interval, but also the weather condition determines the magnitude of these
 119 wind speed and direction variations. In our case the passage of a low pressure system east of Iceland and its warm
 120 front on May 6th, 2013, lead to a change in surface wind direction and an increase in wind speed variations (figure
 121 5). The standard deviation of the LiDAR 10 minute mean wind speeds and directions increase after the passage of a
 122 warm front during the morning hours on May 6th, 2013. This is because turbulence, and with that vertical mixing, is

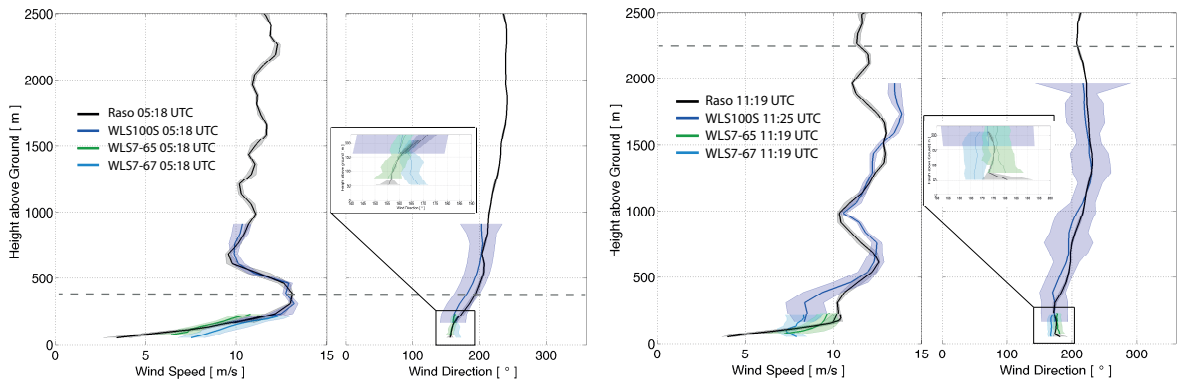


Fig. 5: Vertical profiles of wind speed and direction measured by the three WindCubes and the radiosonde at (a) 05:19 UTC and (b) at 11:19 UTC on May 6th, 2013. Shaded areas indicated the standard deviation of the 10 minutes mean LiDAR profile and of the space averaged radiosonde profile. Lower measurement altitudes are enlarged in the additional boxes. The gray dashed line indicates the boundary layer height estimated from the potential temperature profile measured by the radiosonde

123 enhanced either through an increase in wind shear or due to a positive surface heat flux. The later especially increases
 124 with the approaching cold front of a low pressure system. With enhanced vertical mixing, the planetary boundary
 125 layer depth increases as well, which is reflected in the change in measurement range of the WindCube 100S from 06
 126 to 12 UTC. Therefore we used the LiDAR data availability, which is reflected in the last LiDAR measurement altitude
 127 with a carrier to noise ratio higher than -23 dB, to detect the atmospheric boundary layer height. The estimation of the
 128 boundary layer height by the radiosonde measurements is based on gradients in the potential temperature profile and
 129 is therefore mainly buoyancy dependent. The difference between the two estimates in our case study can be explained
 130 by the vertical wind shear layer above the buoyancy estimated boundary layer height, which still generates turbulence,
 131 leading to a higher LiDAR measurement range. The two different detection methods become closer at noon, as their
 132 difference in boundary layer height estimation is reduced by half.

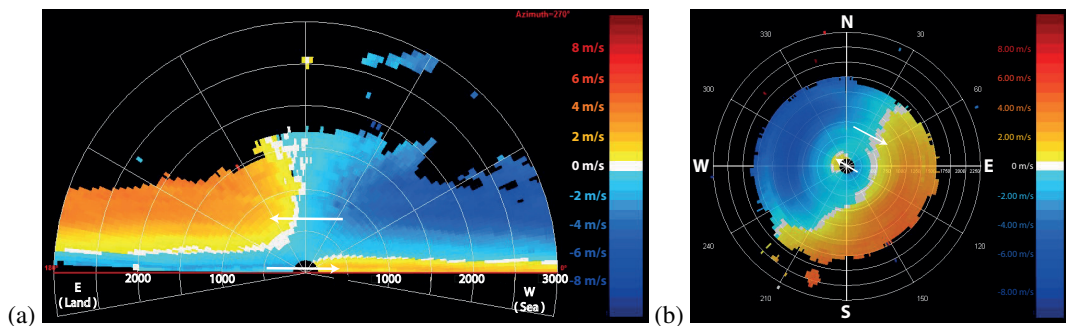


Fig. 6: (a) 180° rhi scan of land breeze from West to East and (b) a 360° PPI scan at 08:30 UTC on March 12th, 2013. Red colors indicate a radial wind speed towards and blue colors away from the device.

133 The second case study is about a land breeze circulation captured with the scanning WindCube 100S on March
 134 12th, 2013. Compared to the sea breeze, the land breeze is less common and most frequent in winter times. On March
 135 12th, 2013 a low pressure system over Scandinavia and a high pressure system south-west of Iceland brought Arctic
 136 air masses from Russia to southern Norway, leading to a distinct temperature gradient between the coast of Norway
 137 and the neighbouring North Atlantic. As the pressure gradient of the synoptic systems was rather low over southern
 138 Norway, the temperature gradient was strong enough to trigger a land breeze circulation. This winter time land breeze
 139 was observed by the scanning WindCube 100S and is illustrated in figure 6. A 180° Range Height Indicator (RHI) scan
 140 pictures a vertical East-West cross section of the above mentioned land breeze. Data is plotted in polar coordinates.

141 Therefore, the two color sets represent the radial wind speeds measured by the WindCube 100S, with blue motion
142 towards the device and red away from it. A clear flow reversal in the first 300 m represents the flow of colder terrestrial
143 air towards the sea, while in higher altitudes air is transported from the sea towards the land. Additionally a more
144 or less horizontal cross section, with a cone angle of 10° , indicates a south-east wind direction and its change with
145 increasing range and height to north west. With 8 m/s at around 1 km above ground the upper layer flow is much
146 stronger compared to 2 m/s at around 200 m. Though, 2 m/s seem to be quite low, this land breeze fits perfectly in the
147 range of land breeze climatologies [2].

148 5. Conclusion

149 First results of LIMECS show an overall good correlation between LiDAR and radiosonde wind measurements
150 above 500 m. Below 500 m the correlation coefficients decrease from $R = 0.99$ to $R = 0.6$. One reason for lower
151 correlation at surface near altitudes can be the pendulum like motion of the sensor on the radiosonde which is triggered
152 when it is released. Since the correlation does not improve after the first measurement heights, where the standard
153 deviations of the radiosonde data minimised, another reasons could be related to local effects that arise with the
154 2.3 kilometre distance between the two measurement sites and an affected performance of the laser amplifier of the
155 WLS7-65. Scanning LiDAR data show potential for boundary layer studies, such as the use of data availability
156 information through the carrier to noise ration can lead to boundary layer height estimation. Additional radial wind
157 speed measurements illustrate nicely boundary layer processes as the land-sea breeze circulation. For this case study,
158 LiDAR measurements follow the theory with a land breeze depth of about 300 m and wind speeds in the order of 2
159 m/s.

160 Acknowledgements

161 The research presented is performed under the Norwegian Center for Offshore Wind Energy (NORCOWE). The
162 authors are grateful to Stig Jone Nevland and all his colleagues from Avinor at Sola airport for opening the roof
163 platform for this measurement campaign and for all their assistance during the measurement period. Special thanks to
164 Inge Nedrebø for his patient solution of network issues and Halvor Vagle and his crew for the helping hand in lifting
165 the LiDARs up and down the rooftop platform. We also would like to thank Kjetil Stiansen and Terje Borge from
166 MET Norway for the organization of the additional radiosonde launches and last but not least Kjell Lea for making
167 the Sola launcher site accessible for us whenever it was needed.

168 References

- 169 [1] M. Courtney R. Wagner, P.L.. Testing and comparison of lidars for profile and turbulence measurements in wind energy. IOP Conference
170 Series: Earth and Environmental Science 2008;1(1):012021. URL: <http://stacks.iop.org/1755-1315/1/i=1/a=012021>.
- 171 [2] Oke, T.R.. Boundary layer climates. Routledge; 1988.
- 172 [3] Steele, C.J., Dorling, S.R., von Glasow, R., Bacon, J.. Idealized wrf model sensitivity simulations of sea breeze types and their effects on
173 offshore windfields. Atmospheric Chemistry and Physics 2013;13(1):443–461. URL: <http://dx.doi.org/10.5194/acp-13-443-2013>.
174 doi:10.5194/acp-13-443-2013.
- 175 [4] Hooper, W.P., Eloranta, E.W.. Lidar measurements of wind in the planetary boundary layer: The method, ac-
176 curacy and results from joint measurements with radiosonde and kytoon. Journal of Climate and Applied Meteorology
177 1986;25(7):990–1001. URL: [http://dx.doi.org/10.1175/1520-0450\(1986\)025<0990:LMOWIT>2.0.CO;2](http://dx.doi.org/10.1175/1520-0450(1986)025<0990:LMOWIT>2.0.CO;2). doi:10.1175/1520-
178 0450(1986)025<0990:LMOWIT>2.0.CO;2.
- 179 [5] Vaisala, . User's Guide; version 3.12 ed. Vaisala; Vaisala Oyj, P.O Box 26, FIN-00421 Helsinki; 2004.
- 180 [6] Vaisala, . Vaisala Radiosonde RS92-SGP. Vaisala; 2013.
- 181 [7] LEOSPHERE, . WINDCUBE Product Information. LEOSPHERE; 2008.
- 182 [8] G. Verroone M. Duboue, G.L.. WINDCUBE100S User Manual; version 1 rev. 11 ed. Leosphere; 2012.
- 183 [9] Martucci, G., Matthey, R., Mitev, V., Richner, H.. Comparison between backscatter lidar and radiosonde measurements of the diurnal
184 and nocturnal stratification in the lower troposphere. Journal of Atmospheric and Oceanic Technology 2007;24(7):1231–1244. URL:
185 <http://dx.doi.org/10.1175/JTECH2036.1>. doi:10.1175/JTECH2036.1.
- 186 [10] Bruce Turner, D.. Comparison of three methods for calculating the standard deviation of the wind direction. Journal of Climate
187 and Applied Meteorology 1986;25(5):703–707. URL: [http://dx.doi.org/10.1175/1520-0450\(1986\)025<0703:COTMFC>2.0.CO;2](http://dx.doi.org/10.1175/1520-0450(1986)025<0703:COTMFC>2.0.CO;2).
188 doi:10.1175/1520-0450(1986)025<0703:COTMFC>2.0.CO;2.